

# Evaluation of Radiation Treatment Planning By Computed Tomography Metal Artifact Reduction Algorithm

Joowan Hong<sup>1</sup>, Jihun Choi<sup>2</sup>, Kyungjin Kim<sup>3</sup>, Jaeouk Ahn<sup>3\*</sup>

1. Department of Radiological sciences, College of Health Sciences, Eulji University, Seongnam-si, Gyeonggi-Do, 13135, Republic of Korea
2. Department of Radiation Oncology, Seoul National University Bundang Hospital, Seongnam-si, Gyeonggi-Do, 13620, Republic of Korea
3. Department of Medical IT Engineering, College of Medical Science, Soonchunhyang University, Asan, Chungnam, 31538, Republic of Korea

ARTICLE INFO	ABSTRACT
<p><b>Article type:</b> Original Paper</p> <p><b>Article history:</b> Received: Sep 29, 2020 Accepted: Dec 09, 2020</p> <p><b>Keywords:</b> Metal Artifact Implants CT Scan Hounsfield Units</p>	<p><b>Introduction:</b> The objective of this study was to evaluate the usefulness of Computed Tomography (CT) images acquired through repeated subtraction reconstruction algorithms to reduce metal artifacts in CT Treatment Planning System (TPS).</p> <p><b>Material and Methods:</b> Origin images of Gammex phantom and Rando phantom and non-orthopedic metal artifact reduction (O-MAR) images were obtained after high density implantation. O-MAR applied images were also obtained. For evaluation of images, regions of interest (ROI) were set at five tissue rods and three points directly affected by artifacts in Gammex phantom. CT number and noise were compared and analyzed. Based on the investigated results using the Gammex phantom, three virtual cylinder target volumes were set on the Rando phantom to dose change of the radiation treatment planning according to the O-MAR. The average dose was then compared and analyzed.</p> <p><b>Results:</b> CT number difference according to the application of O-MAR showed significant difference among lung and bone rod and 3 ROI directly affected. Noise difference according to O-MAR application was significantly different in rod except for bone rod. In the treatment plan using Rando phantom, non-O-MAR and O-MAR images showed -4.3 ~ 1.9% and -0.4 ~ 2.3% dose differences, respectively.</p> <p><b>Conclusion:</b> Applying an O-MAR can reduce image distortion due to high-density implantation, improve image quality, and correct CT numbers.</p>

► Please cite this article as:

Hong J, Choi J, Kim K, Ahn J. Evaluation of Radiation Treatment Planning By Computed Tomography Metal Artifact Reduction Algorithm. Iran J Med Phys 2021; 18: 403-408. 10.22038/IJMP.2020.52418.1864.

## Introduction

Recently, radiation therapy can be accurately and precisely performed due to technological developments. CT images used in radiation treatment planning require high accuracy and precision. At the same time, they can provide anatomical information such as the location and size of the tumor and normal tissues around the tumor. In addition, CT numbers that express differences in attenuation coefficient by tissue enable conversion to the required electron density for radiation dose calculation [1-3]. CT images for accurate radiation treatment planning require accurate anatomical information and CT numbers. High-density artifacts such as titanium rods, gold, and platinum are inserted into teeth implants, vertebrae, and joints, these metal materials can cause large differences in radiation attenuation. These metal artifacts can lead to distortion of the CT image, decreasing the observability of anatomical information and causing changes in CT number of surrounding tissues at the same time [4-6]. Such CT image distortion is likely to affect the calculation of

higher radiation dose more than non orthopedic implants, changed normal tissue and treatment volume, and tumor volume produced in the radiation treatment plan [7-9]. The purpose of this study was to evaluate the usefulness of CT images acquired through repeated subtraction reconstruction algorithms to reduce metal artifacts when CT artifacts were inserted in CT simulations for radiation therapy and radiation planning dose changed.

## Materials and Methods

### Comparison of CT image quality

Gammex phantom (RMI 467, Middleton, WI, USA) was used to compare CT image quality (Figure1). CT image acquisition was performed with a CT simulator (16slice CT, Phillips, Netherlands) with the following conditions for scans: 120 kV tube voltage, 80 mAs tube current time, and 4 mm slice thickness. To obtain the reference origin CT image, each tissue rod was arranged to minimize phantom self-generated artifact.



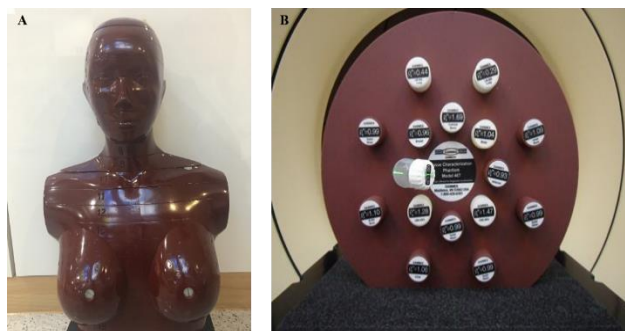


Figure 1. (A) Rando phantom, (B) Gammex phantom

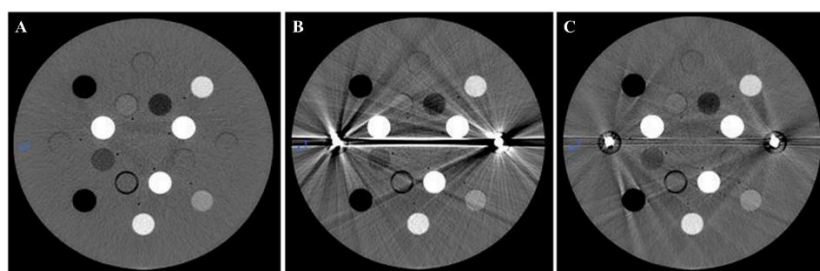


Figure 2. (A) No artifact origin image using Gammex phantom, (B) non applied artifact reduction algorithm image, (C) applied artifact reduction algorithm after metal artifact occurrence.

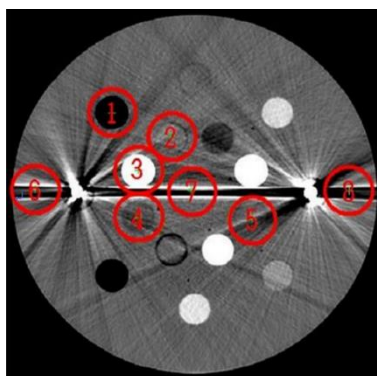


Figure 3. CT number and Noise measurement for regions of interest using Gammex phantom.

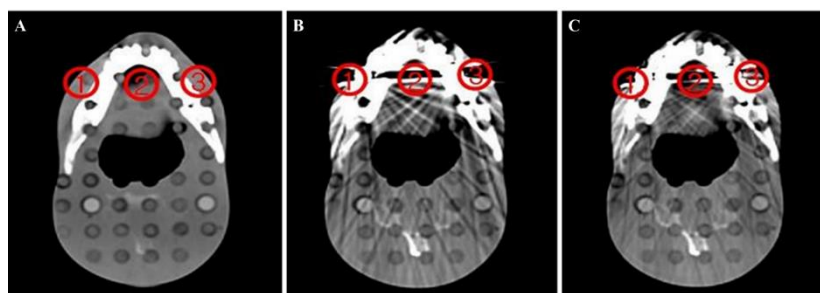


Figure 4. (A) no artifact origin image using Rando phantom, (B) non applied artifact reduction algorithm image, (C) applied artifact reduction algorithm after metal artifact occurrence. 1, 2, 3 was dose measurement ROI.

Also, both sides of the solid water rod of the phantom were replaced with self-produced high-density implants to obtain non O-MAR images. Additional images were obtained after O-MAR application (Figure 2). High density implants were made using self-made

low melting temperature alloy (Cerrobend; Bi 50%, Pb 26.7%, Sn 13.3%, and Cd 10%). Images were acquired five times under the same conditions and eight ROIs were set to analyze CT number and noise based on the original image. ROIs were set at three locations directly

affected by the streak artifact and five locations in the lung, brain, bone, breast, and water rods around the streak artifact (Figure 3). CT numbers and noise for quantitative analysis were calculated with the following formula:

$$CT\ number = \frac{(\mu_{tissue} - \mu_{water})}{\mu_{water}} \times K \quad (1)$$

Where  $\mu_{tissue}$  was linear attenuation coefficient of tissues and  $\mu_{water}$  was linear attenuation coefficient of water and  $K$  was contrast factor.

$$SD(\delta) = \sqrt{\frac{\sum_{i=1}^N (X_i - \bar{X})^2}{N-1}} \quad (2)$$

Where  $N$  was number of total pixels,  $X_i$  was CT number of each pixel, and  $\bar{X}$  was CT number of average of pixels.

### Comparison of radiation therapy dose

Rando phantom was used to obtain radiation therapy dose change according to CT number change of surrounding tissues due to metal artifact. CT image acquisition was performed with a CT simulator (16 slices CT, Phillips, Netherlands) using the following conditions for scans: 120 kV tube voltage, 350 mAs tube current time, and 2 mm slice thickness. An origin CT image was obtained without the insertion of high density implants. A non O-MAR image was obtained after inserting a low melting temperature alloy made in-house on the Rando phantom tooth location. Additionally, an O-MAR applied image was obtained. These three images obtained were constructed with a rods shaped volume at a diameter of 1 cm and a height of 3.2 cm at three locations directly affected by the artifact using a treatment planning system Eclipse (Version 11, Varian, Palo Alto, CA, USA) (Figure 4). The radiation therapy plan applied 6 MV photon beams, 135°, 90°, 45°, 0°, 315°, 270°, 225° gantry angles, field size 15 by 15 cm, and prescription dose of 100cGy. The average dose of the constructed column shaped volume was compared and analyzed based on the origin image.

### Statistical analysis

CT image quality analysis included calculating mean and standard deviation values for each group of ROIs followed by Kruskal-Wallis test and post hoc analysis. All tests with  $p$  values less than 0.05 indicated significant differences. Dose comparisons were performed after calculating percentage differences based on origin images. All statistical analyses were performed using R software version 3.6.0 [10].

## Results

### CT image quality

CT number verification using Gammex phantom showed no significant difference between Rando phantom image and CT number of brain, breast and water rod depending on O-MAR application. Post hoc analysis showed no significant ( $p > 0.05$ ) difference in groups. However, for lung, bone, and three directly affected ROIs, CT numbers showed significant differences. The post-hoc analysis confirmed no significant differences between origin images and O-MAR-applied images, although there were significant ( $p < 0.05$ ) differences between non-O-MAR images and O-MAR-applied images.

The five ROI CT numbers with significant differences were close to the CT number of the Rando phantom origin image when applied to the O-MAR, and the difference was -1.36%, 1.93%, 84.72%, 105.01% and 82.59%, respectively when comparing non-O-MAR and O-MAR CT numbers (Table 1). Noise verification also showed significant ( $p < 0.05$ ) differences for all rods. The post-hoc analysis confirmed no significant difference between the Rando phantom origin image and the non O-MAR image and the O-MAR image ( $p < 0.05$ ). All significant differences of ROI noise levels were reduced after the application of O-MARs, showing improvement of -25.67%, -45.53%, -15.92%, -58.22%, -67.09%, -71.85%, -95.55%, -68.76% in the comparison between non-O-MAR and O-MAR noise for eight ROIs (Table 2).

Table 1. CT number of Gammex phantom ROIs among Origin, Non O-MAR, and O-MAR CT images

Unit: HU				
ROIs	Origin	Non O-MAR	O-MAR	$p$ -value
ROI 1	-715±0.7	-703.4±5.1	-713±2.3	0.004
ROI 2	13.6±0.5	19.6±5.3	14±1.8	0.127
ROI 3	1169.8±1.1	1146±7.2	1168.2±3.1	0.007
ROI 4	-52.6±0.5	-51.6±5.7	-52.2±2.6	0.371
ROI 5	-6.6±0.9	-4.2±7.9	-6.2±3.3	1.000
ROI 6	-3.6±1.5	-121.8±12.4	-18.6±2.9	0.001
ROI 7	-2.2±1.3	-143.6±23.1	7.2±8.0	0.005
ROI 8	-3.6±1.1	-144.8±23.1	-25.2±7.5	0.001

Data are presented as mean ± standard deviation of five replicates ( $n = 5$ ). Values followed by the significantly different (Kruskal Wallis test,  $p < 0.05$ ). ROI: region of interest; ROI1: lung rod; ROI2: brain rod; ROI3: bone rod; ROI4: breast rod; ROI5: water rod; ROI6 to 8: regions directly affected by artifacts.

Table 2. Noise of Gammex phantom ROIs among Origin, Non O-MAR, and O-MAR CT images

ROIs	Origin	Non O-MAR	O-MAR	p-value
ROI 1	10±0.7	14.8±1.3	11±1.0	0.004
ROI 2	10.6±0.5	22.4±2.7	12.2±0.4	0.001
ROI 3	15.8±1.1	22.6±4.4	19±1.9	0.026
ROI 4	10.4±0.5	31.6±3.4	13.2±1.5	0.002
ROI 5	9.8±1.3	46.2±1.9	15.2±0.8	0.001
ROI 6	7.8±2.1	76±8.4	21.4±2.7	0.001
ROI 7	12±1.2	422.8±138.4	18.8±4.3	0.001
ROI 8	7.2±1.1	69.8±11.8	21.8±3.9	0.001

Data are presented as mean ± standard deviation of five replicates (n = 5). Values followed by the significantly different (Kruskal Wallis test, p<0.05). Noise: CT image noise; ROI: region of interest; ROI1: lung rod; ROI2: brain rod; ROI3: bone rod; ROI4: breast rod; ROI5: water rod; ROI6 to 8: regions directly affected by artifacts.

Table 3. Radiation planning dose of Rando phantom

Unit: cGy			
Target	Rando phantom	Non O-MAR	O-MAR
Volume 1	99.7	99.6	97.3
Volume 2	102.1	101.4	102.1
Volume 3	97.0	92.9	99.2

Volume 1: Right side target of Rando phantom, Volume 2 : center target of Rando phantom, Volume 3 : Left side target of Rando phantom.

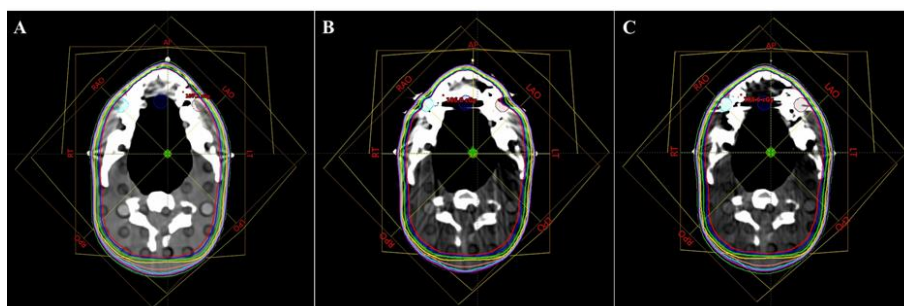


Figure 5. (A) No artifact origin image using radiation planning for Rando phantom, (B) non applied artifact reduction algorithm image, (C) applied artifact reduction algorithm after metal artifact occurrence.

**Radiation therapy dose**

Volume 1 radiation planning dose was 99.7, 99.6, 97.3 cGy in Rando phantom, non O-MAR, and O-MAR. Volume 2 radiation planning dose were 102.1, 101.4, 102.1 cGy in Rando phantom, non O-MAR, and O-MAR. Volume 3 radiation planning dose were 97.0, 92.9, 99.2 cGy in Rando phantom, non O-MAR, and O-MAR. As a result of dose changes in the radiation plan using Rando phantom, non O-MAR and O-MAR image doses were reduced by -0.1% and -2.4%, respectively, with volume 2 showing -0.68% and 0% differences and volume 3 showing -4.22% and 2.26% differences, respectively (Table 3, Figure 5).

**Discussion**

CT images in the radiation treatment planning enable the accurate setting of surface contours, internal structures, and target volumes. In addition, accurate dose calculation can be obtained based on CT numbers for heterogeneous tissues of different body surfaces and densities [11-13]. However, the presence of titanium inserted in dental

implants, vertebrae, and joints in the human body not only causes severe distortion in CT images, but also affects CT numbers of surrounding tissues [14]. Low melting temperature alloy is a material with a density of 9.4 g/cm<sup>3</sup>. It has a density similar to dental amalgam (11.37—13.6 g/cm<sup>3</sup>) and dental gold alloy (10.9—18.7 g/cm<sup>3</sup>). It was chosen as a high density artifact in the present study because it was readily available. Results of this study showed that the O-MAR image in high density artificial peripheral showed a CT number close to that of the original image and the noise was reduced to improve image quality [15].

In addition, dose changes according to CT number changes of surrounding tissues of the metal artifact confirmed that radiation treatment planning using O-MAR applied image was similar to radiation treatment planning using the original image. These results confirmed the usefulness of O-MAR applied CT images in the presence of high density artifacts and the reduction of metal artifacts resulting from CT images obtained by applying O-MAR to patients with dental implants. According to previous research, dose

difference could occur if an inaccurate volume was generated due to the indefinite boundary when generating high-density artificial organs and tumor volume due to metal artifacts [16]. Several previous studies have been conducted to correct metal artifacts caused by high density artifacts in CT images [17-19]. Most studies have focused on reducing image distortion itself for diagnostic purposes [20-23]. However, O-MAR is effective in removing metal artifacts, but limitations cannot restore lost information inside the metal materials [24]. In this study, there was a limitation in that CT images were acquired without metal artifacts of actual patients with tooth implants. However, O-MAR, an algorithm that reduces artifacts by iterative metal sinogram is a way to obtain accurate information about high density artifacts and surrounding tissues during radiation therapy. The application of O-MAR enabled the acquisition of CT images with improved distortion minimization and image quality of high density artificial peripheral tissues. It was useful for calibration of CT number of high density artificial surrounding tissues.

## Conclusion

The accuracy of the radiation planning dose can be improved through accurate volume measurement of tissues and correction of the CT number using O-MAR an iterative reconstruction algorithm.

## Acknowledgment

This research was funded by the Soonchunhyang University Research Fund.

## References

- Li H, Noel C, Chen H, Harold Li H, Low D, Moore K, et al. Clinical evaluation of a commercial orthopedic metal artifact reduction tool for CT simulations in radiation therapy. *Medical physics*. 2012;39(12):7507-17.
- Webster GJ, Rowbottom CG, Mackay RI. Evaluation of the impact of dental artefacts on intensity-modulated radiotherapy planning for the head and neck. *Radiotherapy and Oncology*. 2009;93(3):553-8.
- Coolens C, Childs P. Calibration of CT Hounsfield units for radiotherapy treatment planning of patients with metallic hip prostheses: the use of the extended CT-scale. *Physics in Medicine & Biology*. 2003;48(11):1591.
- Lee C-H, Yun I-H, Hong D-G, Back G-M, Kwon G-T. Evaluation of using Gantry Tilt Scan to Head & Neck of Patients during Radiation Therapy for Reduction of Metal Artifact. *The Journal of Korean Society for Radiation Therapy*. 2010;22(2):85-95.
- Zhao S, Robelton D, Wang G, Whiting B, Bae KT. X-ray CT metal artifact reduction using wavelets: an application for imaging total hip prostheses. *IEEE transactions on medical imaging*. 2000;19(12):1238-47.
- Wellenberg R, Hakvoort E, Slump C, Boomsma M, Maas M, Streekstra G. Metal artifact reduction techniques in musculoskeletal CT-imaging. *European journal of radiology*. 2018;107:60-9.
- Bal M, Spies L. Metal artifact reduction in CT using tissue-class modeling and adaptive prefiltering. *Medical physics*. 2006;33(8):2852-9.
- Matsufuji N, Tomura H, Futami Y, Yamashita H, Higashi A, Minohara S, et al. Relationship between CT number and electron density, scatter angle and nuclear reaction for hadron-therapy treatment planning. *Physics in Medicine & Biology*. 1998;43(11):3261.
- Kovacs DG, Rechner LA, Appelt AL, Berthelsen AK, Costa JC, Friborg J, et al. Metal artefact reduction for accurate tumour delineation in radiotherapy. *Radiotherapy and Oncology*. 2018;126(3):479-86.
- Team RC. R: A language and environment for statistical computing. R Foundation for Statistical Computing, Vienna, Austria. 2012. URL <http://www.R-project.org>. 2018.
- Huang JY, Kerns JR, Nute JL, Liu X, Balter PA, Stingo FC, et al. An evaluation of three commercially available metal artifact reduction methods for CT imaging. *Physics in Medicine & Biology*. 2015;60(3):1047.
- Axente M, Paidi A, Von Eyben R, Zeng C, Bani-Hashemi A, Krauss A, et al. Clinical evaluation of the iterative metal artifact reduction algorithm for CT simulation in radiotherapy. *Medical physics*. 2015;42(3):1170-83.
- Andersson KM, Nowik P, Persliden J, Thunberg P, Norrman E. Metal artefact reduction in CT imaging of hip prostheses – an evaluation of commercial techniques provided by four vendors. *The British journal of radiology*. 2015;88(1052):20140473.
- M Safdari, A Karimian, M Reza Yazdchi. A new method for metal artifact reduction in CT scan images. *Iranian Journal of Medical Physics*. 2013;10(2):139-146
- Shim E, Kang Y, Ahn JM, Lee E, Lee JW, Oh JH, et al. Metal artifact reduction for orthopedic implants (O-MAR): usefulness in CT evaluation of reverse total shoulder arthroplasty. *American Journal of Roentgenology*. 2017;209(4):860-6.
- Healthcare P. Metal artifact reduction for orthopedic implants (O-MAR). White Paper, Philips CT Clinical Science, Andover, Massachusetts. 2012.
- Joemai RM, de Bruin PW, Veldkamp WJ, Geleijns J. Metal artifact reduction for CT: Development, implementation, and clinical comparison of a generic and a scanner-specific technique. *Medical physics*. 2012;39(2):1125-32.
- Lewis M, Toms AP, Reid K, Bugg W. CT metal artifact reduction of total knee prostheses using angled gantry multiplanar reformation. *The Knee*. 2010;17(4):279-82.
- Rim J, Choi J-A, Lee SA, Khil EK. Comparison of metal artifact reduction for orthopedic implants versus standard filtered back projection: value of postoperative CT after hip replacement. *Journal of the Korean Society of Radiology*. 2018;78(1):22-9.
- Gillet R, Teixeira P, Bonarelli C, Coudane H, Sirveaux F, Louis M, et al. Comparison of radiographs, tomosynthesis and CT with metal artifact reduction for the detection of hip prosthetic loosening. *European radiology*. 2019;29(3):1258-66.

21. Boos J, Sawicki LM, Lanzman RS, Thomas C, Aissa J, Schleich C, et al. Metal artifact reduction (MAR) based on two-compartment physical modeling: evaluation in patients with hip implants. *Acta Radiologica*. 2017;58(1):70-6.
22. Wuest W, May M, Brand M, Bayerl N, Krauss A, Uder M, et al. Improved image quality in head and neck CT using a 3D iterative approach to reduce metal artifact. *American Journal of Neuroradiology*. 2015;36(10):1988-93.
23. Golden C, Mazin SR, Boas FE, Tye G, Ghanouni P, Gold G, et al. A comparison of four algorithms for metal artifact reduction in CT imaging. *Physics of Medical Imaging*. 2011;12(30)
24. PAUDEL, Moti Raj, et al. Clinical evaluation of normalized metal artifact reduction in kVCT using MVCT prior images (MVCT-NMAR) for radiation therapy treatment planning. *International Journal of Radiation Oncology\* Biology\* Physics*. 2014;89(3):682-689